ELSEVIER

Journal of Nuclear Materials 248 (1997) 19–26

journal of nuclear materials

Section 2. Hydrogen isotope behavior in graphitic and ceramic materials

Carbon chemistry due to combined H^+ and O^+ irradiation

A.A. Haasz [a,*], Allen Y.K. Chen [a], J.W. Davis [a], E. Vietzke [b]

[a] *Fusion Research Group, University of Toronto Institute for Aerospace Studies, 4925 Dufferin Street, North York, Ontario, Canada M3H 5T6*

[b] *Institut für Plasmaphysik, Forschungszentrum (KFA) Jülich, Association Euratom-KFA, D-52425 Jülich, Germany*

Abstract

An investigation of carbon chemistry due to simultaneous H^+ and O^+ impact of pyrolytic graphite is presented. As an introduction, an overview is given of previous results related to the chemical erosion processes of graphite due to single-species impact by hydrogen and oxygen. Some limited previous synergistic results of various multispecies impact studies of graphite are also presented. In the present investigation, pyrolytic graphite (Union Carbide HPG99) was exposed to 5 keV O^+ and 1 keV H^+, resulting in a 10–20% reduction of CO and CO_2 erosion yields (in comparison with the O^+-only case) for flux ratios of $\phi_{O^+}/\phi_{H^+} \sim 6$–27%. Maximum CO and CO_2 reduction was observed at ~ 800 K graphite temperature. In addition, water production was observed with a maximum of ~ 0.15 H_2O/O^+ at ~ 800 K. Only a small reduction (~ 5–10%) in the methane yield (CH_4/H^+) was seen. © 1997 Elsevier Science B.V.

1. Introduction

Graphite is one of the prime candidates for use as a first-wall material in future fusion devices. Its excellent thermomechanical properties enable the material to withstand the high plasma heat loading inside fusion reactors, and its low-Z reduces the effect of fuel dilution and plasma cooling. Unfortunately, in addition to physical sputtering, graphite shows regimes of enhanced erosion at elevated temperatures: it can be eroded by radiation-enhanced sublimation (RES) and by chemical reactions due to hydrogen and oxygen impact. While physical sputtering and RES require a threshold energy for the incident ions (~ 20–30 eV for light ion impact), chemical erosion can occur with low-energy ions or thermal atoms and cannot be avoided by lowering the plasma temperature near the plasma-facing material.

Chemical erosion in fusion reactors with carbon or carbon-based materials results mainly from reactions between carbon and the hydrogenic fuel or the oxygen plasma impurity, leading to the formation of hydrocarbons, carbon monoxide, and carbon dioxide. Water formation is also possible in the complex C–O–H system. These processes are further complicated by other multispecies impact phenomena involving the addition of the C impurity and He ash to the impacting species. Carbon atoms due to physical sputtering or RES, or hydrocarbon molecules due to chemical erosion, from the carbon-containing first-wall may be ionized (and dissociated in the case of C_xH_y molecules) within the plasma and find their way back to the wall. We note that some of the implanted particles will be trapped and thus affect tritium inventory, fuel recycling, and microstructure. Comprehensive recent reviews of these topics are available: erosion [1,2]; hydrogen transport/retention/re-emission [3,4]. In addition to the plasma particles, neutrons are also present in D–T burning reactors, and via impact with materials, can lead to changes in material characteristics, and consequently affect plasma–materials interaction (PMI) behavior.

Most PMI phenomena have been extensively studied in the laboratory for single species, and in some cases for combined species impact. However, almost no data exist currently on the effect of exposing graphite simultaneously to energetic oxygen and energetic hydrogen. With our dual-beam accelerator facility we are in a unique position to investigate such a reaction system, and the new results

* Corresponding author. Tel.: +1-416 667 7717; fax: +1-416 667 7743; e-mail: aahaasz@utias.utoronto.ca.

0022-3115/97/$17.00 © 1997 Elsevier Science B.V. All rights reserved.
PII S0022-3115(97)00112-8

presented here are based on such a study. However, as a prelude to the present work, we shall present a brief overview of previous investigations of single-species H and O impact on carbon as well as some multispecies impact studies.

2. Overview of previous investigations

2.1. Chemical erosion of carbon due to hydrogen

The flux of hydrogenic plasma particles striking plasma-facing components will primarily be in the form of ions, charge-exchange neutrals, and Franck–Condon neutrals, with energies ranging from a few eV to keV's. From controlled laboratory experiments, a comprehensive database exists for chemical erosion involving sub-eV neutral hydrogen atoms, H^0, (simulating the Franck–Condon neutrals) and energetic (> 100 eV) H^+ impacting on various forms of graphite. The energy range between sub-eV and ~ 100 eV has not been extensively investigated in previous laboratory experiments using ion beams, mainly because of beam flux limitations in this range. However, recent developments with gaseous divertors in tokamaks have led to the achievement of few-eV plasma-edge temperatures, resulting in H impact energies as low as ~ 10 eV. Consequently, plasma-materials interaction studies have recently shifted emphasis to energies < 100 eV. The controlling reaction parameters are the energy and flux of the impacting particles, and the temperature and microstructure of the graphite specimens.

2.1.1. Chemical erosion due to thermal hydrogen atoms

Molecular hydrogen of thermal energy does not react with graphite [5], but thermal H^0 impact on carbon materials results in the formation of CH_3, CH_4 and a wide spectrum of heavier hydrocarbons, with the latter dominating the total erosion yield [6–9]. The temperature dependence of the steady-state hydrocarbon yield in the H^0–C reaction is characterized by a maximum occurring at about 550–600 K [9]. The maximum yields can vary by as much as a factor of 2 for fine grain and poorly oriented pyrolytic graphites [10], but the temperature at which the maximum yield occurs (T_m) remains relatively constant, except for a slight flux dependence [8]. At T_m, the measured absolute methane yields are in the range 10^{-4}–10^{-3} $CH_{3,4}/H^0$ [8,11], and the total carbon erosion is about 10^{-3} to 5×10^{-3} C/H^0 [9].

2.1.2. Chemical erosion due to energetic hydrogen ions

When graphite is bombarded with energetic hydrogen ions, the formation of an H-saturated amorphous near-surface layer occurs, with a depth corresponding to the ion range [12–15]. Essentially, the implanted hydrogen atoms are trapped near the end of their trajectory. As the hydrogen concentration becomes saturated in the implantation zone (reaching a value of 0.4 H/C at room temperature, and decreasing with increasing irradiation temperature [16–18]), re-emission of hydrogen and the formation of volatile hydrocarbons are observed. For H^+ energies in the range 100 eV–10 keV, the steady-state total hydrocarbon production rates are more than an order of magnitude larger than the thermal H^0–C case, and the hydrocarbon spectrum produced also differs from the H^0 irradiation case. Unlike the H^0 case where the chemical erosion is dominated by heavy hydrocarbon, the H^+-induced spectrum is dominated by methane, with only smaller amounts of C_2H_x and C_3H_y molecules being observed. At T_m, the contribution of the C_2 and C_3 groups to the total C erosion is relatively small for high H^+ energies (roughly 15% at 1 keV), but becomes more significant at low energies (roughly 45% at 100 eV) [9,19].

The key fusion-relevant parameters associated with chemical erosion of graphite due to H^+ impact are the incident particle energy, flux and target temperature. The effects of energy and temperature are shown in Fig. 1. For energies > 300 eV, erosion yield maxima occur at about 750–850 K [5,9,19]. In the case of CH_4, a maximum yield of about 0.07 CH_4/H^+ is observed for H^+ energies between 300 eV and 1 keV; the total chemical erosion at

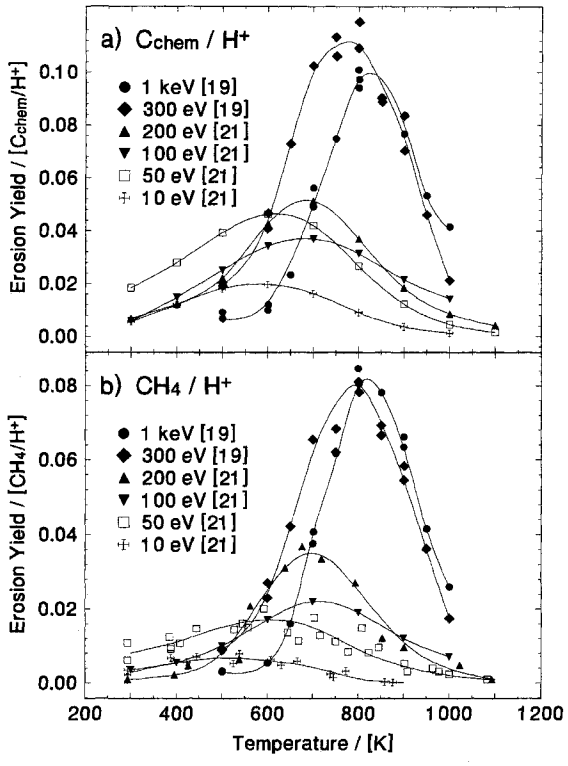

Fig. 1. Temperature dependence of erosion yields of CH_4 and C_{chem} ($C_{chem} = CH_4$ yield plus heavy hydrocarbon yields) due to H^+ impact on graphite at various irradiation energies (10–200 eV [21], and 300 eV–1 keV [19]).

T_m, including heavier hydrocarbons and methane, is ~ 0.1 C/H^+. In the less-explored energy range of few eV to 200 eV, two significant observations are made [20–22]. First, as the energy decreases, the yield maximum Y_m for methane formation decreases and the position of the maximum, i.e., T_m, shifts to lower temperatures. Second, the heavy hydrocarbon fraction of the total chemical erosion yield increases with decreasing energy [21]. As far as isotopic effects are concerned, for temperatures up to 800 K methane yields due to D^+ are higher than those due to H^+ by factors ranging from < 2 [21] to 5 [23]. The reason for this wide variation is not evident.

The third key parameter which might affect hydrocarbon production is the incident H^+ or D^+ flux. From a compilation of erosion yields obtained in both ion-beam experiments and plasma experiments in fusion devices [24], for ~ 100 eV H^+ or D^+ impact energies, due to the scatter of the data, no clear flux dependence of the erosion yield can be discerned.

Experiments aimed at identifying the mechanistics of the hydrocarbon formation/release process came to the conclusion that hydrocarbons are formed in the graphite at the end of the incident-ion range [6,25–29]. As the detached hydrocarbon molecule diffuses towards the front surface of the material, it can undergo fragmentation due to incident ions [30,31]. The fact that lower-energy incident ions lead to hydrocarbon formation in a shallow surface layer (i.e., shorter range and hence shorter diffusion length for the molecule and less probability of fragmentation) is consistent with the observation that lower-energy ions lead to relatively more heavy-hydrocarbon release.

2.2. Chemical erosion of carbon due to oxygen

Oxygen is often the main intrinsic impurity in the plasmas of current fusion devices. Some results on the interaction of oxygen with carbon materials have been compiled in Refs. [2,5]. Molecular-beam experiments with $O_2 \rightarrow$ graphite at temperatures above 1000 K have produced a maximum yield of about 2 to 5×10^{-3} CO/O_2 at 1300–1500 K and at least an order of magnitude smaller CO_2 yield [32–34]. In comparison, the reactivity of atomic oxygen is much higher (a factor of ~ 40 at 1400 K) than that of O_2, even at low temperatures [35–37]. Here we will concentrate on ionic oxygen as it is more relevant to fusion devices.

The interaction of energetic oxygen ions with graphite leads to a complex process of implantation, trapping, chemical reaction and re-emission, somewhat similar to the $H^+ \rightarrow C$ interaction discussed above. Implanted oxygen from bombarding O^+ ions is trapped or re-emitted in the form of CO or CO_2, as in the case of thermal oxygen [32]. No re-emitted O or O_2 has been found. For O^+ energies above 500 eV, the adsorption and complex formation rate is near unity [32]. With increasing O^+ fluence, the implanted oxygen is partly retained and the release of CO and CO_2 increases steadily until the trapped oxygen concentration in the carbon reaches a saturation value of ~ 0.25 O/C at room temperature [38–40]; the saturation level decreases with increasing carbon temperature, again similar to the case of hydrogen ion impact. After saturation is reached, all of the newly implanted oxygen ions react to form CO or CO_2. At room temperature, the CO molecules released were found to have an energy distribution with two components: about 60% of CO molecules are released with a thermal energy distribution characteristic of the target temperature, while the remaining 40% is released by an activated process (molecular sputtering) and have energies in the 0.25 eV range [40,41].

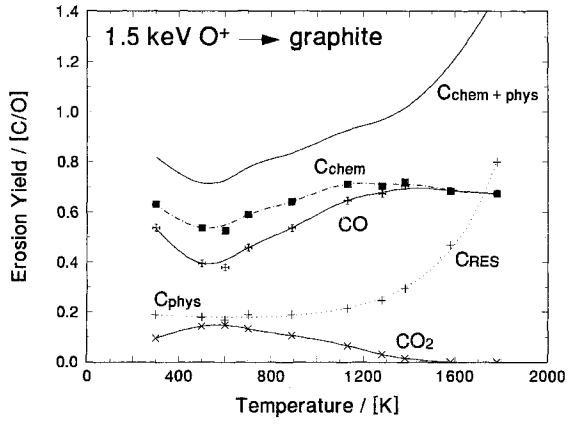

Fig. 2. Temperature dependence of the erosion yields of graphite exposed to 1.5 keV O^+ [40,41].

Fig. 2 shows the temperature dependence of the various erosion yields for graphite exposed to 1.5 keV O^+ [40,41]. The CO formation yield, as well as the total chemical erosion yield (C_{chem} in Fig. 2), show a slight temperature dependence with a minimum at ~ 600 K. The yield for CO_2, however, has a maximum at roughly the same temperature and vanishes for temperatures above 1400 K. The total C erosion yield (sum of chemical erosion and physical sputtering) is nearly temperature-independent and has a value between 0.7 and unity for temperatures below 1000 K and incident O^+ energies above 500 eV [32,42,43]. Above 1200 K the contribution from RES becomes important. The energy dependence of the reaction yield for CO and CO_2 was observed to be weak in the O^+ energy range of 50 eV to a few keV's [32,44]. Below 50 eV, however, a decreasing trend is observed [44].

2.3. Synergistic erosion of carbon due to multispecies impact

In addition to the deuterium and tritium fuel and the fusion reaction products (He and neutrons), the fusion edge plasma that comes in contact with materials also contains

impurities that are produced via PMI (e.g., C and O), and may contain other gas species that are deliberately introduced in the plasma in order to control the edge plasma itself (e.g., Ar or Ne used in radiatively cooled gaseous divertors). Here, we shall limit our discussion only to *simultaneous* (as opposed to *sequential*) impact by various combinations of two plasma species. From laboratory ion-beam experiments, the temperature-dependence profiles of hydrocarbon formation for (H^+ & H^0) [45–47], (Ar^+ & H^0) [11], (C^+ & H^0) [48] and (C^+ & H^+) [49,50] were found to be similar to the H^+-only case, with a maximum production rate at about 750–800 K. Other results obtained for nonreactive energetic (~ 1 keV) He^+, Ne^+ and Ar^+, in conjunction with low energy (< 100 eV) H^+, show enhancements of the erosion yield, [50], indicating an increase of the near-surface damage due to the addition of energetic ions. Typically, the addition of energetic ions on the order of a few percent of the H^+ (< 100 eV) flux appears to be sufficient to increase the total chemical erosion yield to ~ 0.1 C/H^+ (which is the maximum yield produced by 300 eV–1 keV H^+ ions alone).

In the case of (O^+ & H^0), in addition to hydrocarbon formation, CO is also generated, and the reaction rate for CO formation is near unity even at room temperature [51]. In a recent experiment with a mixed 5 keV D_2^+ and $^{18}O^+$ ion beam, water (D_2O) molecules were also formed in addition to methane, CO, and CO_2 [52]. The D_2O exhibits the same temperature dependence as methane, reaching a maximum at ~ 800 K. Other results, involving combined energetic H^+ and thermal O_2 irradiation on graphite, show that the production of CO and H_2O does not affect the yield and temperature dependence of hydrocarbon formation [53].

The reactivity of thermal O_2 on graphite is also enhanced by simultaneous Ar^+ and O_2 impact [32]. In addition to the high-temperature branch for CO formation observed for $O_2 \rightarrow C$ impact (see Section 2.2 above), a low temperature branch, near room temperature, exists for both CO and CO_2, the latter being about an order of magnitude smaller. The associated temperature dependence of the low-temperature branch is similar to the oxygen surface concentration during O^+ impact on graphite [32].

The object of the present investigation is to analyze the reaction products formed during simultaneous bombardment of graphite with independently controlled beams of H^+ and O^+ ions. In contrast to most of the experiments described above, where an enhancement in C-erosion was observed, a synergistic reduction in C-erosion is expected in the present case, due to the formation of water.

3. Current experiment

3.1. Apparatus

The erosion of graphite has been studied under conditions of simultaneous bombardment by 10 keV O_2^+ (5 keV/O^+) and 3 keV H_3^+ (1 keV/H^+) ions, using an independently controlled high-flux, low-energy, mass-analyzed dual-beam ion accelerator system [50]. From previous studies of methane formation from graphite under H^+ and H_3^+ irradiation, the H_3^+ molecular ion was found to behave effectively as three H^+ ions with one-third of the H_3^+ ion energy [45]. Thus it is assumed that the incident O_2^+ and H_3^+ molecular ions break up immediately into atoms upon impact with the specimen. The respective ion energies were chosen to produce the maximum ion fluxes and the maximum amount of implantation overlap. The two beams intersected in the target chamber with a 42° angle of separation, and the target specimen was normally placed at the point of intersection such that the beams were 21° from the surface normal; see Fig. 3. Fluxes were in the range $0.9–3 \times 10^{19}$ O^+/m^2 s, and $0.9–2 \times 10^{20}$ H^+/m^2 s, with flux ratios being $\phi_{O^+}/\phi_{H^+} \sim 6–27\%$. The beam spots, slightly elliptical in shape due to the off-normal incidence, were ~ 5 mm (for H^+) and ~ 4.5 mm (for O^+) in diameter. This allowed complete overlapping of the O^+ beam spot by the H^+ spot at the focus. The specimen was a strip of 'as-deposited' pyrolytic graphite (HPG99 from Union Carbide) with a density of ~ 2200 kg/m^3, and approximate dimensions of $50 \times 10 \times 0.4$ mm^3, with the central portion sanded down to a thickness of ~ 0.1 mm. It was held by stainless steel jaws to allow direct current heating, and was biased at $+30$ V to suppress secondary electrons.

The target chamber was baked for at least 24 h at ~ 500 K before the experiments, and the specimen was

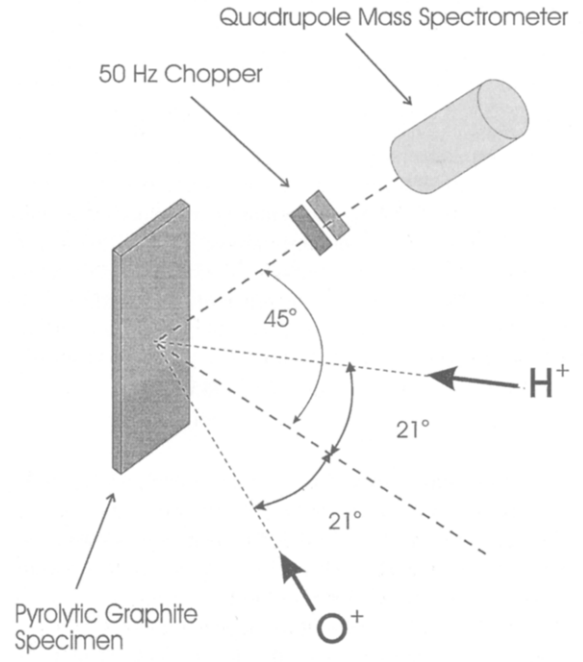

Fig. 3. Schematic diagram of the apparatus configuration in the vacuum chamber.

heated to ~ 1500 K in situ before performing each experiment at a specific temperature. Reaction products were measured by both residual gas analysis (RGA) and direct line-of-sight (LOS) quadruple mass spectrometry (QMS) over the temperature range 400 to 1200 K. A computer-controlled data acquisition system was used to collect QMS data. The specimen temperature was monitored with an optical pyrometer.

For RGA the absolute erosion yields of methane, carbon monoxide and carbon dioxide were obtained by using commercially produced calibrated leaks with an absolute error of 20%. The absolute value of the water production rate (O–H–C reaction) was estimated from the maximum reduction in the total oxygen balance at ~ 800 K by comparing the O–C and O–H–C reactions. For direct line-of-sight measurements, CH_4, CO and CO_2 yields were scaled to the calibrated RGA data, while water production was estimated from the CO data taking into account the different ionization cross-sections and quadruple transmission sensitivities of CO and water.

3.2. Results and discussion

The raw trace of a typical experimental run in the RGA mode (at 800 K) is presented in Fig. 4. As shown, the experiment consisted of four phases. Only the O^+ beam was turned on during the first phase, then the H^+ beam was added in the second phase. For the third phase, the O^+ beam was turned off, while the H^+ beam remained on. The fourth phase was a measure of the background with no beams on. The CO, CO_2, and H_2O yields, corresponding to O^+ and H^+ simultaneous exposures were obtained from the differences between the phase II and phase III signals, the latter being the effective background (H^+-induced signals coming from the chamber walls, etc.); i.e.,

$$Y^i_{II} = K^i\left(S^i_{II} - S^i_{III}\right)/\phi_{O^+},$$

where Y^i is the yield for species i, K^i is the corresponding calibration factor, S^i is the measured QMS signal, and ϕ_{O^+} is the O^+ flux. We confirmed the wall origin of the effective background signals in separate experiments where the specimen was irradiated by H^+ only (and Ar^+ only) prior to exposure to O^+. Similarly, the yields corresponding to O^+-only exposure were obtained from

$$Y^i_{I} = K^i\left(S^i_{I} - S^i_{IV}\right)/\phi_{O^+}.$$

For the evaluation of the CH_4 yield, an analogous procedure was followed, however, $S^{CH_4}_{I}$ is now the effective background for the (O^+ and H^+) yield, and signals are normalized by the H^+ flux. The same procedures were followed for the experiments in the LOS mode.

Fig. 5 shows the temperature dependence of CO, CO_2 and H_2O yields measured in the RGA mode. The total oxygen released ($CO + 2CO_2$ in the O^+-only case and $CO + 2CO_2 + H_2O$ in the (O^+ & H^+) case) is also plotted. In addition, Refke's RGA results of 3 keV O_2^+ (i.e., 1.5 keV/O) impact on EK98 (fine grain isotropic graphite from Ringsdorff) [41] are included for comparison. For the O^+-only case, the CO yield temperature profile has a shallow minimum at ~ 700 K, and the yields (present results) range from 0.6 to 0.9 CO/O^+. The temperature profile is similar to that of Refke's RGA results, except our yield at the minimum is about a factor of 2 higher. The CO_2 profile has a shallow maximum at ~ 700 K and the agreement between the present results and those of Refke is quite good. The maximum CO_2 yield is smaller than the CO yield at the corresponding temperatures by about a factor of 5. With both the H^+ and O^+ beams turned on, a ~ 10–20% drop in both the CO and CO_2 production is observed. In addition, water production is observed with a maximum yield of ~ 0.15 H_2O/O^+, also at about 800 K.

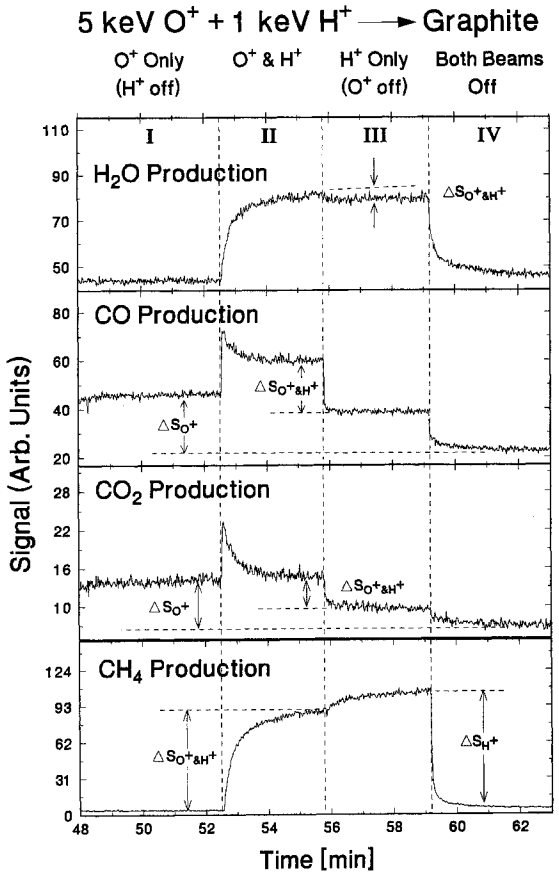

Fig. 4. Typical raw traces of the QMS signals of H_2O, CO, CO_2 and CH_4 in the RGA detection mode during 5 keV O^+ and 1 keV H^+ bombardment of graphite at 800 K. The traces are divided into four phases: (I) O^+ beam only; (II) simultaneous O^+ and H^+ irradiation; (III) H^+ beam only; and (IV) both beams turned off. Signal magnitudes due to single-beam only and dual-beam irradiation for each species are indicated.

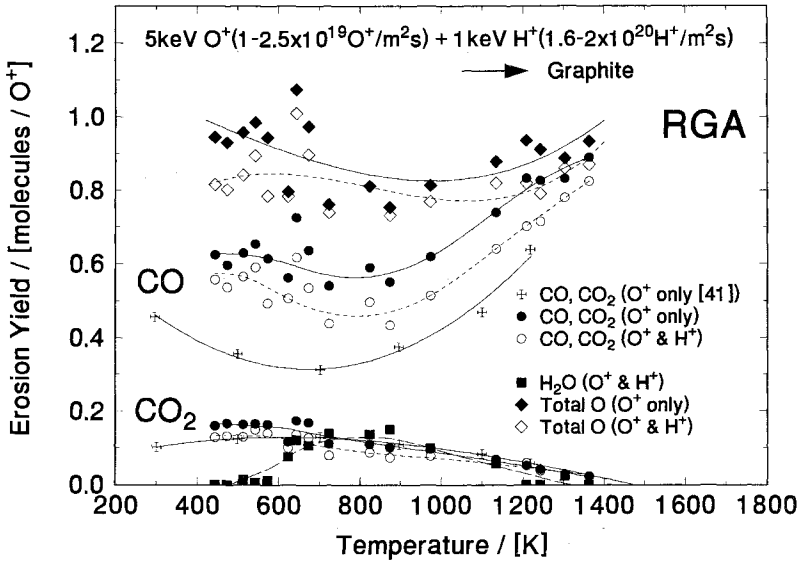

Fig. 5. Temperature dependence of CO, CO_2 and H_2O yields, measured in the RGA mode, due to 5 keV O^+ ($1–2.5 \times 10^{19}$ O^+/m^2 s) and 1 keV H^+ ($1.6–2 \times 10^{20}$ H^+/m^2 s) on HPG99. Total oxygen released ($CO + 2CO_2$) is also plotted. For comparison, RGA results of CO and CO_2 yields measured in the RGA mode for 3 keV O^+ impact on EK98 graphite are also included [41].

The total oxygen released for both O^+-only and (O^+ & H^+) cases is between 0.8 and unity. The scatter of data in Fig. 5, especially at low temperatures (< 700 K), is attributed to transient effects, i.e., at lower temperatures relatively longer times are needed for the QMS signals to reach steady-state. Finally, only a small (~ 5–10%) reduction in the methane yield is seen when O^+ is added to the H^+ irradiation (less than 10% at 800 K); see Fig. 6.

The reason for performing the experiments in the line-of-sight QMS detection mode was to substantially suppress any non-beam related background signals (for example, the CO and CO_2 signals observed during H^+-only bombardment in RGA experiments). However, two important drawbacks of the LOS–QMS technique are (i) low signals, and (ii) not having in-situ absolute calibration. Nevertheless, low signal problems could be overcome by using longer

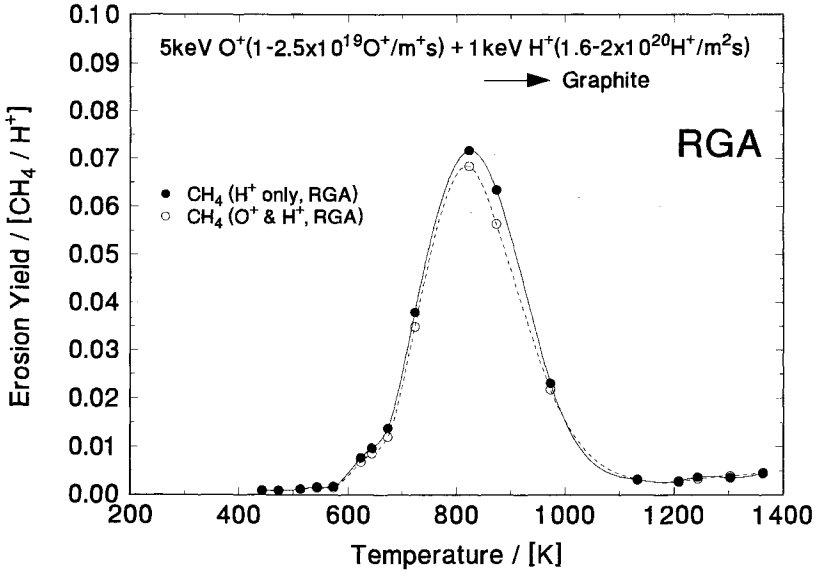

Fig. 6. Temperature dependence of CH_4 yields, measured in the RGA mode, due to 5 keV O^+-only ($1–2.5 \times 10^{19}$ O^+/m^2 s) and combined 5 keV O^+ and 1 keV H^+ ($1.6–2 \times 10^{20}$ H^+/m^2 s) on HPG99.

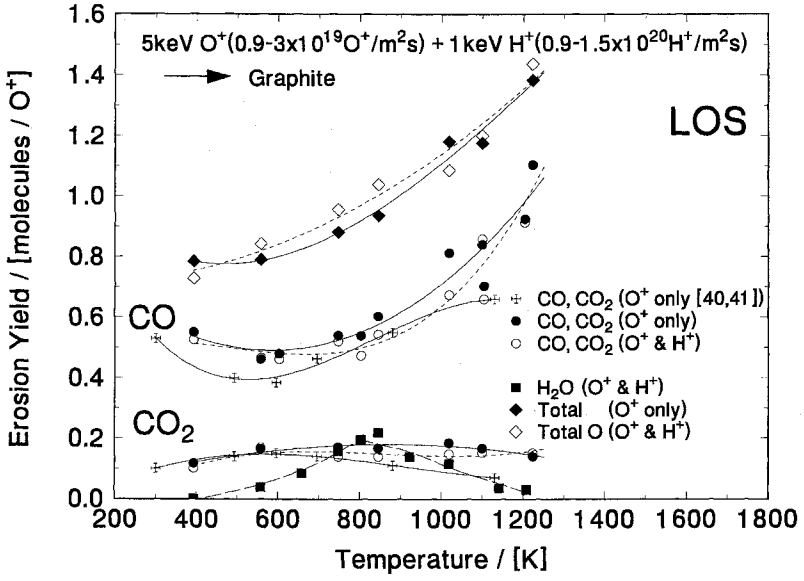

Fig. 7. Temperature dependence of CO, CO_2 and H_2O yields, measured in the LOS mode, due to 5 keV O^+ ($0.9–3 \times 10^{19}$ O^+/m^2 s) and 1 keV H^+ ($0.9–1.5 \times 10^{20}$ H^+/m^2 s) on HPG99. Total oxygen released ($CO + 2CO_2$) is also plotted. For comparison, LOS results of CO and CO_2 yields measured in the LOS mode for 1.5 keV O^+ impact on HPG99 graphite are also included [40,41].

detection times and absolute yields could be obtained by setting a particular data point (or the average of a set of points) to the corresponding absolute value on the RGA plot. In the present study the LOS yield curves were set to correspond to the RGA data (Fig. 5) at ~ 750 K.

The LOS results are presented in Fig. 7. Here too, previously published results for the O^+-only case [40,41] are included for comparison. Due to the non-thermal nature of the energies of some of the released CO during irradiation [40,41], which is not taken into consideration in the present analysis, the actual shape of the LOS profiles will be different. In fact, this may be the cause of the greater-than-unity value of the total oxygen yield, $(CO + 2CO_2)/O^+$, for temperatures above 900 K. Since exact partition of the energies of the released particles is only known for room temperature and there are indications that it varies with temperature [40,41], more time-of-flight results will be needed to obtain more accurate temperature profiles for the LOS data.

Except for higher temperatures (> 800 K), the temperature profiles of CO and CO_2 yields for the O^+-only case are similar to the RGA data and the LOS results of 1.5 keV $O^+ \rightarrow$ HPG99 from Ref. [40,41]. For $T > 800$ K, the yields for CO and CO_2 in the LOS mode are slightly higher. The nature of the discrepancy is not known. In the simultaneous O^+ and H^+ case, a slightly smaller reduction in CO and CO_2 yields (compared to the RGA results) are observed. This may be due to the intrinsic low signal-to-noise ratio in our LOS detection. Furthermore, as in the RGA mode, water is also observed in the (O^+ & H^+) case. The maximum yield for water is slightly higher, likely due to a different method of estimating the absolute yield, but the temperature dependence is identical.

4. Conclusion

During simultaneous bombardment of graphite by 5 keV O^+ and 1 keV H^+, with H^+ fluxes higher than O^+ fluxes by factors of ~ 5–10, only ~ 10–20% reduction is observed for both the CO and CO_2 yields over the entire temperature range. Corresponding to the slightly reduced $O^+ \rightarrow C$ reactivity, a small amount of water production (~ 0.15 H_2O/O^+ at 800 K) is observed with a temperature dependence similar to that of CH_4 formation. Finally, under the conditions of the present experiments, the O^+ flux appears to have only a small influence on the production of CH_4. The reduction of CO, CO_2 and CH_4 yields and the water formation yield are all of the same order of magnitude, and are about an order of magnitude lower than the total oxygen release rate.

Acknowledgements

This work was supported by the Canadian Fusion Fuels Technology Project and the Natural Sciences and Engineering Research Council of Canada. E.V.'s visit to the Toronto laboratory was supported by EURATOM (Staff Mobility). Thanks are also extended to Charles Perez for his help with the preparation of the apparatus.

References

[1] W. Eckstein, V. Philipps, in: Physical Processes of the Interaction of Fusion Plasmas with Solids, eds. W.O. Hofer and J. Roth (Academic Press, Amsterdam, 1996) p. 93.

[2] E. Vietzke, A.A. Haasz, in: Physical Processes of the Interaction of Fusion Plasmas with Solids, eds. W.O. Hofer and J. Roth (Academic Press, Amsterdam, 1996) p. 135.

[3] J.K. Ehrenberg, in: Physical Processes of the Interaction of Fusion Plasmas with Solids, eds. W.O. Hofer and J. Roth (Academic Press, Amsterdam, 1996) p. 35.

[4] A.A. Haasz, P. Franzen, J.W. Davis, S. Chiu, C.S. Pitcher, J. Appl. Phys. 77 (1) (1995) 66.

[5] J. Roth, E. Vietzke, A.A. Haasz, Suppl. Nucl. Fusion 1 (1991) 63.

[6] E. Vietzke, K. Flaskamp, V. Philipps, J. Nucl. Mater. 128& 129 (1984) 545.

[7] A.A. Haasz, O. Auciello, P.C. Stangeby, J. Vac. Sci. Technol. 32 (1986) 1179.

[8] A.A. Haasz, J.W. Davis, J. Chem. Phys. 85 (1986) 3293.

[9] J.W. Davis, A.A. Haasz, P.C. Stangeby, J. Nucl. Mater. 155–157 (1988) 234.

[10] V. Philipps, K. Flaskamp, E. Vietzke, J. Nucl. Mater. 122& 123 (1984) 1440.

[11] E. Vietzke, K. Flaskamp, V. Philipps, J. Nucl. Mater. 111& 112 (1982) 763.

[12] J. Roth, R.A. Zuhr, S.P. Withrow, W.P. Eatherly, J. Appl. Phys. 63 (1988) 2603.

[13] R. Siegele, J. Roth, B.M.U. Scherzer, S.J. Pennycook, J. Appl. Phys. 73 (1993) 1988.

[14] K. Niwase, M. Sugimoto, T. Tanabe, F.E. Fujita, J. Nucl. Mater. 155–157 (1988) 303.

[15] K.N. Kushita, K. Hojou, Ultramicroscopy 35 (1991) 289.

[16] J. Roth, B.M.U. Scherzer, R.S. Blewer, D.K. Brice, S.T. Picroux, W.R. Wampler, J. Nucl. Mater. 93&94 (1980) 601.

[17] W.R. Wampler, D.K. Brice, C.W. Magee, J. Nucl. Mater. 102 (1981) 304.

[18] M. Braun, B. Emmoth, J. Nucl. Mater. 128&129 (1984) 657.

[19] A.A. Haasz, J.W. Davis, J. Nucl. Mater. 175 (1990) 84.

[20] C.H. Wu, J.W. Davis, A.A. Haasz, 'The formation of methane by the interaction of very low energy hydrogen ions with graphite', Proc. 15th Euro. Conf. on Contr. Fusion and Plasma Heating, Dubrovnik, Europhysics Conference Abstracts, 1988, p. 691.

[21] B.V. Mech, A.A. Haasz, J.W. Davis, J. Nucl. Mater. 241–243 (1997) 1147.

[22] A.A. Haasz, B.V. Mech, J.W. Davis, J. Nucl. Mater. 231 (1996) 170.

[23] J. Roth, J. Bohdansky, Nucl. Instrum. Methods B23 (1987) 549.

[24] J.W. Davis, A.A. Haasz, J. Nucl. Mater. 241–243 (1997) 37.

[25] W. Möller, B.M.U. Scherzer, Appl. Phys. Lett. 50 (1987) 1870.

[26] J. Roth, J. Bohdansky, Appl. Phys. Lett. 51 (1987) 964.

[27] R. Yamada, J. Appl. Phys. 67 (1990) 4118.

[28] S. Chiu, A.A. Haasz, J. Nucl. Mater. 196–198 (1992) 972.

[29] S. Chiu, A.A. Haasz, J. Nucl. Mater. 208 (1994) 282.

[30] S. Chiu, A.A. Haasz, P. Franzen, J. Nucl. Mater. 218 (1995) 319.

[31] A.A. Haasz, S. Chiu, P. Franzen, J. Nucl. Mater. 220–222 (1995) 815.

[32] E. Vietzke, T. Tanabe, V. Philipps, M. Erdwes, K. Flaskamp, J. Nucl. Mater. 145–147 (1987) 425.

[33] D.R. Olander, W. Siekhaus, R.H. Jones, J.A. Schwarz, J. Chem. Phys. 57 (1972) 408.

[34] D.R. Olander, R.H. Jones, J.A. Schwarz, W. Siekhaus, J. Chem. Phys. 57 (1972) 421.

[35] G.R. Hennig, in: Chemistry and Physics of Carbon, ed. P.L. Walker (Dekker, New York, 1996) Vol. 2, p. 1.

[36] M. Otterbein, L. Bonnetain, Comput. Rend. 259 (1964) 791.

[37] D.E. Rosner, H.D. Allendorf, Heterogeneous Kinetics at elevated Temperatures, Proc. Int. Conf. Univ. Pennsylvania 1969 (Plenum, New York, 1970) p. 231.

[38] W.R. Wampler, O.K. Brice, J. Vac. Sci. Technol. A4 (1986) 1186.

[39] A. Refke, V. Philipps, E. Vietzke, M. Erdweg, J. von Seggern, J. Nucl. Mater. 212–214 (1994) 1255.

[40] E. Vietzke, A. Refke, V. Philipps, M. Hennes, J. Nucl. Mater. 220–222 (1995) 249.

[41] A. Refke, PhD thesis, Forschungszentrum Jülich, Univ. Düsseldorf (1994).

[42] E. Hechtl, J. Bohdansky, J. Roth, J. Nucl. Mater. 103&104 (1981) 333.

[43] E. Hechtl, J. Bohdansky, J. Nucl. Mater. 122&123 (1984) 1431.

[44] In Ref. [2].

[45] A.A. Haasz, J.W. Davis, O. Auciello, P.C. Stangeby, E. Vietzke, K. Flaskamp, V. Philipps, J. Nucl. Mater. 145–147 (1987) 412.

[46] R. Yamada, K. Sone, J. Nucl. Mater. 98 (1981) 167.

[47] R. Yamada, K. Sone, J. Nucl. Mater. 120 (1984) 119.

[48] J.W. Davis, A.A. Haasz, Appl. Phys. Lett. 57 (1990) 1976.

[49] J.W. Davis, A.A. Haasz, C.H. Wu, J. Nucl. Mater. 196–198 (1992) 581.

[50] A.A. Haasz, J.W. Davis, Nucl. Instrum. Methods B83 (1993) 117.

[51] J. Roth, W. Ottenberger, Max Plack Institut für Plasmaphysik, Garching (1990), unpublished.

[52] E. Vietzke, V. Philipps, KFA Forschungszentrum, Jülich (1990), unpublished; presented in Ref. [3].

[53] A.A. Haasz. J.W. Davis, University of Toronto (1990) unpublished.